Theoretical study of the electronic states of AlB

Charles W. Bauschlicher, Jr. and Stephen R. Langhoff
NASA Ames Research Center, Moffett Field, California 94035

(Received 7 February 1994; accepted 21 March 1994)

The singlet, triplet, and quintet states of AlB below about 30 000 cm^{-1} are studied theoretically to facilitate spectroscopic investigations and for comparison with analogous calculations on the Al_2 and B_2 molecules. The ground state of AlB is $X\ ^3\Sigma^-$ with a dissociation energy of 1.96±0.06 eV. The $A\ ^3\Pi$ state is computed to lie only 610 cm^{-1} above the ground state. Since transitions from the $(2)^3\Sigma^-$ state to both the $X\ ^3\Sigma^-$ and $A\ ^3\Pi$ states are predicted to be relatively strong, these transitions in the region of 17 000–18 000 cm^{-1} should be an excellent means of characterizing AlB and of determining the $X-A$ separation. The adiabatic ionization potential to form the $X\ ^2\Sigma^+$ ground state of AlB^+ is estimated to be 7.05 eV. Overall the spectroscopy of AlB is much more similar to Al_2 than B_2.

I. INTRODUCTION

The spectroscopy of jet-cooled Al_2 has now been well characterized by resonant two-photon ionization spectroscopy[1] and laser-induced fluorescence.[2] More recently, several new electronic transitions of the B_2 molecule were observed by Brazier and Carrick[3] in emission from a corona excited supersonic expansion source. For both molecular systems, the assignment of the experimental spectra was facilitated by comparison with high-level *ab initio* calculations.[4,5] In contrast, to our knowledge the AlB molecule has not been studied previously either theoretically or experimentally. It is the purpose of this paper to characterize the spectroscopy of AlB at the same level as for Al_2 and B_2 to facilitate future spectroscopic studies of this molecule. It is also of interest to compare AlB with Al_2 and B_2. Alloys can have very different properties from those of its components, and these differences can manifest themselves even for diatomic systems. For example, the binding energy of YNi (2.904±0.001 eV)[6] is significantly larger than that of either Y_2 (1.62±0.22 eV)[7] or Ni_2 (2.068±0.010 eV).[8] In this case there is a significant enhancement in the strength of the bonding through donation of d electrons from the "d-rich" Ni atom to the "d-poor" Y atom.[9] Although we do not expect such dramatic effects for simple metals, it is still of interest to determine whether the properties of AlB are intermediate to those of Al_2 and B_2.

A significant difference in the spectroscopy of AlB compared with the component homonuclear systems is expected due to the fact that more transitions are dipole allowed as a result of the loss of g and u symmetry. For example, transitions from a common upper state, such as $(2)^3\Sigma^-$, can be used to determine spectroscopically the small energy difference between the $X\ ^3\Sigma^-$ and $A\ ^3\Pi$ states. The fact that the $X\ ^3\Pi_u$ and $A\ ^3\Sigma_g^-$ states of Al_2 have different g and u symmetries precludes the use of a transition from a common upper state to determine the very small energy difference between these states. There is also the possibility of strong transitions in AlB that have no analog in the homonuclear systems, such as charge transfer states that are observed,[10] for example, for CuAg, but not for Cu_2 or Ag_2.

The fact that the Al and B atoms both have $^2P^o(s^2p^1)$ ground states, leads to two triplet states, $^3\Pi(s^2s^2p\sigma^1p\pi^1)$ and $^3\Sigma^-(s^2s^2p\pi^2)$ with comparable energies. For Al_2, the ground state is $^3\Pi_u$ by about 200 cm^{-1},[11] while for B_2 the $A\ ^3\Pi_u$ state lies more than 3000 cm^{-1} higher than the $X\ ^3\Sigma_g^-$ ground state.[5] As evidenced by the significantly larger dissociation energy of B_2 (Ref. 5) than Al_2 (Ref. 1) and the much larger cohesive energy of boron than Al metal,[12] the bonding between the more compact boron atoms is stronger than between aluminum atoms. Another manifestation of the stronger bonding is the presence of a low-lying $^5\Sigma_u^-(s^2s^1p\sigma^1p\pi^2)$ state ($T_e\approx1700$ cm^{-1}) for B_2, while this state lies above 12 000 cm^{-1} for Al_2. There are also significant differences in the potential curves for many of the excited states. In this work we study the spectroscopy of AlB to facilitate spectroscopic studies and to contrast it with the homonuclear systems.

II. METHODS

Three different Gaussian orbital basis sets are used in this work. For our study of the spectroscopy of AlB we employ the atomic natural orbital (ANO) basis sets of Widmark *et al.*[13] These sets can be denoted as: Al $(17s12p5d4f)/[5s4p2d1f]$ and B $(14s9p4d3f)/[4s3p2d1f]$. Basis set completeness is assessed by comparing the spectroscopic constants for the $X\ ^3\Sigma^-$ and $A\ ^3\Pi$ states computed with this one-particle basis with those using the more complete correlation-consistent-valence polarized quadruple-zeta and quintuple-zeta (cc-pVQZ or cc-pV5Z) sets of Dunning and co-workers.[14,15] Only the pure spherical harmonic components of the basis functions are used.

The orbitals are optimized using both a single state and a state-averaged (SA) complete-active-space self-consistent-field (CASSCF) approach. More extensive correlation is then added using the multireference configuration-interaction (MRCI) approach. All configurations in the CASSCF wave function are used as references in the MRCI calculations. The contribution from higher excitations is estimated using the multireference analog of the Davidson correction, denoted $+Q$, and the averaged coupled-pair functional (ACPF) approach.[16] We used the internal contraction (IC) procedure[17] to keep the CI calculations tractable. The calcu-

TABLE I. Calibration calculations for the two lowest states of AlB and AlB^+.

	$X\ ^3\Sigma^-$			$A\ ^3\Pi$		
AlB	$r_e(a_0)$	$\omega_e(cm^{-1})$	$D_e(eV)$	$r_e(a_0)$	$\omega_e(cm^{-1})$	$T_e(cm^{-1})$
ANO ICMRCI	3.895	593	1.84	4.238	483	617
ANO ICMRCI+Q	3.898	592	1.84	4.243	482	392
ANO ICACPF	3.897	592	1.84	4.242	482	453
cc-pVQZ ICMRCI	3.861	599	1.92	4.201	487	757
cc-pVQZ ICMRCI+Q	3.863	598	1.92	4.206	485	539
cc-pV5Z ICMRCI	3.856	610	1.94	4.196	496	772
cc-pV5Z ICMRCI+Q	3.857	608	1.94	4.201	494	552
cc-pV5Z ICACPF	3.857	609	1.94	4.199	494	610
AlB^+		$X\ ^2\Sigma^+$			$A\ ^2\Pi$	
ANO ICMRCI	5.201	245	0.78	4.472	296	3334

lations are performed using the MOLPRO code[17,18] on the NAS Facility CRAY C90 computer and the Computational Chemistry IBM RS/6000 computers.

The $^4P(2s^12p^2)$ state of B is 28 800 cm^{-1} above the $^2P^\circ(2s^22p^1)$ ground state.[19] The next excited state is about 12 000 cm^{-1} higher in energy. The $^2S(3s^24s^1)$, $^4P(3s^13p^2)$, and $^2D(3s^23d^1)$ states of Al are 25 000, 29 000, and 32 400 cm^{-1} above the $^2P^\circ(3s^23p^1)$ ground state, respectively. However, because the $4s$ orbital is very diffuse, the molecular states derived from the Al ^2S state are expected to be only weakly bound. Therefore, the low-lying states of AlB should be derived from the $^2P^\circ + {}^2P^\circ$, $^2P^\circ + {}^4P$, and $^4P + {}^2P^\circ$ asymptotes. Hence, the active space was chosen to include the valence s and p orbitals, which corresponds in C_{2v} symmetry to a (4220) CASSCF treatment. While all the states derived from these three asymptotes were included in the preliminary SA-CASSCF procedure, the highest states were removed from the final SA-CASSCF calculations. For the triplet and singlet manifolds, 10 of the 18 possible states were included, while for the quintet manifold 8 of the possible 12 states were included. The most significant limitation of these calculations is the exclusion of the Al $3d$ orbital from the active space. As discussed in our Al_2 paper,[4] this active space could underestimate the contribution of the Al ^2D asymptote to the higher lying states, and thus these states might be described less accurately than the lower states.

In this work, we compute Einstein A coefficients (in s^{-1}), which can be defined as

$$A_{v'v''}=2.026\times10^{-6}g\tilde{\nu}^3_{v'v''}|D_{v'v''}|^2, \tag{1}$$

where $\tilde{\nu}_{v'v''}$ is the transition energy in cm^{-1} between v' of the upper state and v'' of the lower state, $D_{v'v''}$ is the electronic transition moment between the v' and v'' levels and g is a statistical weighting factor, equal to two for $\Sigma\rightarrow\Pi$ transitions and one for all others. The $D_{v'v''}$ values are computed numerically using a spline representation of the ICMRCI potentials and transition moments. Note that rotationless potentials are used throughout, but the influence of vibration–rotation interactions on the lifetimes is rather small. The radiative lifetime ($\tau_{v'}$) of a vibrational level depends on the sum of the transition probabilities to all lower vibrational levels in all lower electronic states. If rotational effects are neglected, the lifetime can be written as

$$\tau_{v'}=\left(\sum_{v''}A_{v'v''}\right)^{-1}. \tag{2}$$

A simplified procedure was used for bound-free emission, which involved replacing $\tilde{\nu}^3_{v'v''}$ and $|D_{v'v''}|^2$ in Eq. (1) by the vertical energy separation for $v'=0$ and 1 and transition moment at r_0' and r_1'. The accuracy of this simplified procedure depends on the shape of the transition moment function. For the bound–bound transitions where the moment is smooth and does not change sign in the Franck–Condon region, this approximation agrees with the results from Eq. (1) to within a few percent. The poorest agreement is found for the $(2)^3\Sigma^-\rightarrow X\ ^3\Sigma^-$ transition, where the transition moment changes sign near $r_e'\approx r_e''$. In this case the approximate formula yields an A value that is a factor of 30 too small. Because none of the bound-free transition moments change sign near r_e', this simplified approach should account quantitatively for the relatively small bound-free contribution to the lifetimes.

III. SEPARATE STATE CALCULATIONS FOR THE LOW-LYING STATES OF AlB AND AlB^+

In this section, we describe a series of calibration calculations for the two low-lying triplet states of AlB, with the goal of providing the most accurate values possible for the spectroscopic constants and the $X\ ^3\Sigma^- - A\ ^3\Pi$ separation. In addition, we want to determine an economical means of studying the higher electronic states, where some compromises in the theoretical approach are required. To obtain the most accurate spectroscopic constants we optimize the orbitals separately for the $X\ ^3\Sigma^-$ and $A\ ^3\Pi$ states using a (4220) active space. The ICMRCI and ICACPF results in the three basis sets described in the previous section are summarized in Table I.

Higher excitations increase slightly the bond length of both states, decrease the $T_e(A\ ^3\Pi)$ value by $\approx$200 cm^{-1}, and have essentially no effect on either D_e or ω_e. Since these effects are small, we do not report $+Q$ corrections for the higher-lying excited states. Improving the basis set in-

TABLE II. Spectroscopic constants for the electronic states of AlB computed using the SA-CASSCF/ICMRCI method and ANO basis.

State	$r_e(a_0)$	$\Delta G_{1/2}(\text{cm}^{-1})$	$T_e(\text{cm}^{-1})$
$X\ ^3\Sigma^-$	3.893	588	0
$A\ ^3\Pi$	4.234	481	523
$(1)^1\Delta$	3.964	540	4207
$(1)^1\Sigma^+$	4.553	314	4872
$(1)^1\Pi$	4.304	442	5264
$(1)^5\Sigma^-$	3.720	736	8823
$(2)^1\Sigma^+$	4.305	508	8867
$(1)^3\Delta$		repulsive[a]	
$(2)^3\Sigma^-$	3.873	520	17787
$(1)^3\Sigma^+$		repulsive	
$(2)^3\Pi$		repulsive[b]	
$(1)^1\Sigma^-$		repulsive	
$(3)^3\Pi$	3.921	882	23383
$(2)^3\Delta$	4.123	729	23455
$(2)^3\Sigma^+$	4.101	673	25434
$(3)^3\Sigma^-$	3.865	691	25453
$(2)^1\Delta$	4.162	465	25716
$(2)^1\Pi$		repulsive	
$(3)^1\Pi$	3.633	718	26731
$(1)^5\Delta$	4.161	531	27867
$(1)^5\Sigma^+$	4.177	523	28566
$(2)^5\Sigma^-$	4.334	460	29135
$(3)^1\Sigma^+$	4.210	442	30768
$(2)^1\Sigma^-$	3.868	746	30826
$(1)^5\Pi$	3.972	549	31288
$(2)^5\Pi$		repulsive	

[a]At this level of theory there is a very shallow well at $r=4.08\ a_0$, which is 17 010 cm^{-1} above the ground state—see Fig. 1.
[b]At this level of theory there is a very shallow well at $r=3.69\ a_0$, which is 20 241 cm^{-1} above the ground state—see Fig. 1.

creases the T_e value and decreases the r_e values slightly. The dissociation energy increases with basis set improvement. The D_e value of 1.94 eV obtained with the cc-pV5Z basis is probably still at least 0.02 eV from the basis set limit. We also expect that inner-shell correlation will increase D_e slightly. On the basis of comparable calculations for Al_2 and B_2 and the experimental value for Al_2, we estimate D_0 for AlB to be 1.96±0.06 eV, which is very close to the average of the results for Al_2 (1.34±0.06 eV)[1] and B_2 (2.85±0.06 eV).[5] Our best T_e value (610 cm^{-1}) is obtained at the ACPF level in the cc-pV5Z basis set. The uncertainties in T_e are sufficiently small that the ground state can be definitively assigned as $X\ ^3\Sigma^-$. By taking one half the error in the r_e values of our best valence treatments of Al_2 and B_2 compared with experiment, we estimate that the true r_e value for the $X\ ^3\Sigma^-$ state of AlB is about 3.81 a_0. Most of the difference between this value and our best calculated value is due to inner-shell correlation effects.

For our study of the higher-lying excited states of AlB, we have for reasons of economy used the ANO basis sets. Compared with the very complete cc-pV5Z basis, this introduces errors of approximately 0.04 a_0 in r_e, 16 cm^{-1} in ω_e and 0.1 eV in D_e for the $X\ ^3\Sigma^-$ state spectroscopic constants and about 150 cm^{-1} in the T_e for the $A\ ^3\Pi$ state. A comparison of the single state results in Table I with the state-averaged results in Table II shows that the use of state averaging in the CASSCF introduces very small errors in the spectroscopic constants and about 100 cm^{-1} in $T_e(A\ ^3\Pi)$.

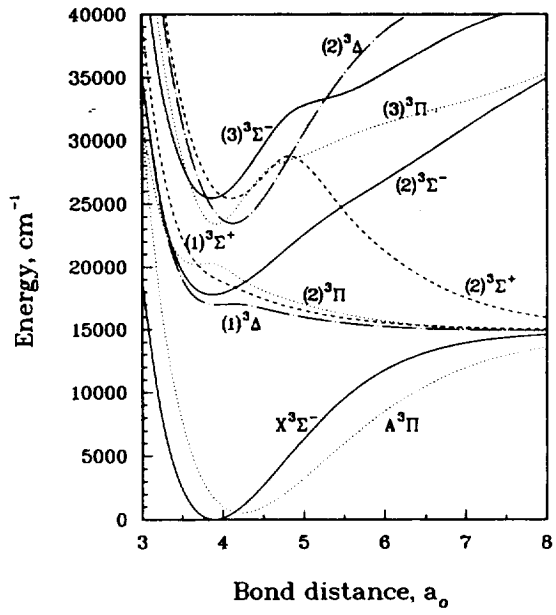

FIG. 1. Potential energy curves for the triplet states of AlB. The $^3\Sigma^-$ states are denoted by solid lines, the $^3\Pi$ states by dotted lines, the $^3\Delta$ states by dot–dashed lines, and the $^3\Sigma^+$ states by the dashed lines.

We feel that these errors are sufficiently small that the SA-CASSCF/ICMRCI approach in the ANO basis will give realistic potential curves for the higher-lying states.

To study AlB using resonant two-photon ionization spectroscopy, it is necessary to have an estimate for the ionization potential (IP). Using the ANO basis set and an analogous treatment of electron correlation, we studied the two lowest doublet states of AlB^+—see Table I. The ground state is $X\ ^2\Sigma^+$, in analogy with Al_2^+ (Ref. 20) and B_2^+ (Ref. 21). The $A\ ^2\Pi$ state is calculated to lie slightly more than 3300 cm^{-1} higher at this level of treatment. The r_e for the $X\ ^2\Sigma^+$ state is considerably longer than the $A\ ^2\Pi$ state, because it has one more σ electron. With only one bonding electron, AlB^+ is significantly less bound than AlB and the $X\ ^2\Sigma^+$ and $A\ ^2\Pi$ r_e values are both significantly longer than those of the neutral states. The directly computed IP of 6.95 eV, is expected to be too small considering the error in the calculated IP of Al atom. Using the experimental IP[19] of Al to position the asymptotes yields our best estimate of 7.05 eV for the adiabatic IP of AlB.

IV. THE HIGHER-LYING STATES OF AlB

The triplet, singlet, and quintet states are plotted in Figs. 1–3, respectively, and the spectroscopic constants are summarized in Table II. A comparison with the analogous potential energy curves for Al_2 and B_2 shows that AlB has a greater similarity to Al_2. For example, the $^3\Sigma^- - ^3\Pi$ separation of 523 cm^{-1} is much closer to Al_2 (−227 cm^{-1}) than B_2 (3380 cm^{-1}). Another indication is that the $^5\Sigma^-$ state lies 8823 cm^{-1} above the ground state for AlB compared with 1833 cm^{-1} for B_2 and 12 317 cm^{-1} for Al_2. The $(1)^3\Delta_u$, $(1)^3\Sigma_u^+$, $(1)^3\Pi_g$, and $(1)^1\Sigma_u^-$ states are all bound for B_2 and repulsive for Al_2. For AlB the corresponding states are

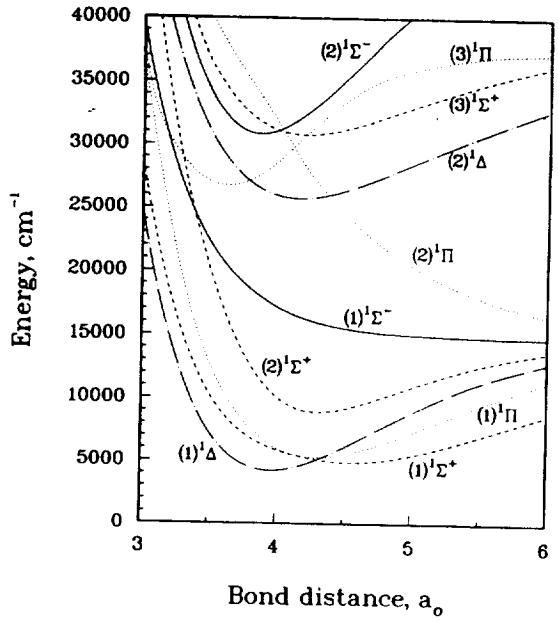

FIG. 2. Potential energy curves for the singlet states of AlB. The $^1\Sigma^-$ states are denoted by solid lines, the $^1\Pi$ states by dotted lines, the $^1\Delta$ states by dot–dashed lines, and the $^1\Sigma^+$ states by the dashed lines.

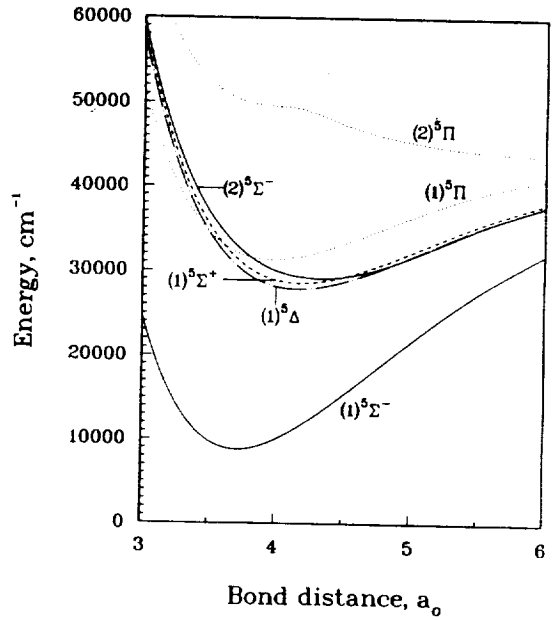

FIG. 3. Potential energy curves for the quintet states of AlB. The $^5\Sigma^-$ states are denoted by solid lines, the $^5\Pi$ states by dotted lines, the $^5\Delta$ state by dot–dashed line, and the $^5\Sigma^+$ state by the dashed line.

largely repulsive, with the $(1)^3\Sigma^+$ and $(1)^3\Delta$ states having very shallow wells lying above the asymptote. Thus, while AlB has properties intermediate between Al_2 and B_2, it is more similar to Al_2.

The variation in r_e values of the electronic states of AlB can be related to their principal occupations. While the $A\ ^3\Pi(s^2s^2p\sigma^1p\pi^1)$ and $X\ ^3\Sigma^-(s^2s^2p\pi^2)$ states both have a bond order of one, the extra σ electron results in an r_e value that is 0.34 a_0 longer for the $A\ ^3\Pi$ state. The $(1)^1\Pi$ state has the same occupation as the $A\ ^3\Pi$ state, but has a smaller binding energy and larger r_e value due to the loss of exchange energy. The $(1)^1\Delta$ state is derived from the same occupation as the $X\ ^3\Sigma^-$ state and therefore has a relatively short bond length. The $(1)^1\Sigma^+$ state is dominated by the $s^2s^2p\pi^2$ occupation at shorter r values and by the $s^2s^2p\sigma^2$ occupation at longer r values. The avoided crossing that occurs between the $(1)^1\Sigma^+$ and $(2)^1\Sigma^+$ states is similar to that observed for Al_2. The bond lengths for both $^1\Sigma^+$ states are substantially longer than the $(1)^1\Delta$ state due to the contribution to both states from the $s^2s^2p\sigma^2$ occupation where all of the electrons are in the σ space. The $^5\Sigma^-(s^2s^1p\sigma^1p\pi^2)$ state has one of the shortest bond lengths of any of the states considered, as a consequence of having a bond order of 1.5 and two electrons in the $p\pi$ orbital. The higher lying states tend to have longer bond lengths due to the partial occupation of the $2\pi^*$ orbital. One notable exception is the

TABLE III. The lifetime of each excited state and contribution (reported as $1.0/\Sigma A_v$) to this lifetime from each lower state. Decay to the $X\ ^3\Sigma^-$, $A\ ^3\Pi$, and $(2)^2\Sigma^-$ states is computed rigorously, while the contributions from the repulsive $(2)^3\Pi$, $(1)^3\Sigma^+$, and $(1)^3\Delta$ states are computed using the approximate formula (see the text).

		Contributions (μs)					
Upper state	Total lifetime (μs)	$X\ ^3\Sigma^-$	$A\ ^3\Pi$	$(2)^3\Sigma^-$	$(2)^3\Pi$	$(1)^3\Sigma^+$	$(1)^3\Delta$
$v'=0$							
$(2)^3\Sigma^-$	14.704	32.820	26.640				
$(2)^3\Sigma^+$	0.335		0.356		15.358	8.843	
$(3)^3\Pi$	0.595	2.328	0.880	14.620	222.398	134.377	29.298
$(2)^3\Delta$	0.297		0.307		38.729		6.316
$(3)^3\Sigma^-$	0.208	0.620	0.330	6.374	108 235.0		
$v'=1$							
$(2)^3\Sigma^-$	6.392	8.172	29.340				
$(2)^3\Sigma^+$	0.327		0.378		10.102	6.400	
$(3)^3\Pi$	0.382	2.524	0.481	13.250	99.334	69.784	23.324
$(2)^3\Delta$	0.304		0.317		63.643		8.681
$(3)^3\Sigma^-$	0.182	0.447	0.324	6.710	14 649.0		

TABLE IV. Franck–Condon factors for decay from the $v'=0$ level of the upper states to the $A\ ^3\Pi$ and $X\ ^3\Sigma^-$ states.

		$A\ ^3\Pi$						$X\ ^3\Sigma^-$	
Upper state	v''	0	1	2	3	4	5	0	1
$(2)^3\Sigma^-$		0.127	0.207	0.209	0.167	0.117	0.074	0.994	0.003
$(2)^3\Sigma^+$		0.713	0.251	0.034	0.001	0.000	0.000		
$(3)^3\Pi$		0.120	0.254	0.273	0.196	0.103	0.040	0.966	0.012
$(2)^3\Delta$		0.747	0.233	0.018	0.000	0.000	0.000		
$(3)^3\Sigma^-$		0.071	0.167	0.215	0.199	0.148	0.094	0.975	0.024

$(3)^1\Pi(s^2s^1p\pi^3)$ state, which has three bonding $p\pi$ electrons.

The small energy separation and large difference in the r_e values of the $X\ ^3\Sigma^-$ and $A\ ^3\Pi$ states results in a long radiative lifetime of 0.21 s for the $v'=0$ level of the $A\ ^3\Pi$ state. Therefore this band system is probably more amenable to absorption rather than emission studies. The transition moment of about 0.35 a.u. in the Franck–Condon region results in a modest (greater than 4×10^{-5}) oscillator strength for the $0\leftarrow0$, $1\leftarrow0$, and $2\leftarrow0$ transitions. That is, the intensity of these transitions are comparable to that of a strong (greater than 100 km/mol) vibrational transition. Hence, it may be possible to directly measure the $^3\Sigma^- - ^3\Pi$ separation for AlB, whereas the very small separation in Al_2 has to date precluded a direct measurement. However, observing emission to these low-lying states from a common upper state offers another attractive possibility of accurately determining this state separation.

The radiative lifetimes for the $v'=0$ and 1 levels of all bound triplet states lying between about 17 000–26 000 cm^{-1} are summarized in Table III. We have also decomposed the lifetimes into their individual components to identify the strongest band systems. The bound-free contribution is computed using our approximate procedure, but never makes a substantial contribution to the lifetimes for $v'=0$ or 1. The Franck–Condon factors for decay from the $v'=0$ level of these states are given in Table IV. This work clearly identifies several band systems that should be readily observable spectroscopically. We consider these band systems in detail.

The $(2)^3\Sigma^-$ state is dipole connected to both the $X\ ^3\Sigma^-$ and $A\ ^3\Pi$ states, and both transitions are reasonably strong. Although the $(2)^3\Sigma^-$ and $X\ ^3\Sigma^-$ states have similar r_e values, the $(2)^3\Sigma^-\rightarrow X\ ^3\Sigma^-$ transition is not dominated by a $\Delta v=0$ sequence, because the electronic transition moment changes sign very near r_e (see Table V, where the transition moments at 3.8, 4.0, and 4.2 a_0 are tabulated). This results in stronger transitions for $2\rightarrow0$ and $1\rightarrow0$ than $0\rightarrow0$, and likewise stronger transitions for $1\rightarrow0$ and $1\rightarrow2$ than $1\rightarrow1$. The large difference in bond lengths between the $A\ ^3\Pi$ and $(2)^3\Sigma^-$ states results in several strong transitions for the $(2)^3\Sigma^-\rightarrow A\ ^3\Pi$ band system. This is well illustrated by the Franck–Condon factors in Table IV. The lifetime of the $v'=0$ level is 14.7 μs and is determined almost equally by decay to the $X\ ^3\Sigma^-$ and $A\ ^3\Pi$ states, while the lifetime of the $v'=1$ level is determined predominantly by decay to the $X\ ^3\Sigma^-$ state—see Table III. The $(2)^3\Sigma^-$ state is crossed near r_e by the repulsive $(1)^1\Sigma^-$ state, which is mostly of $s^2s^2p\pi^1p\pi^{*1}$ parentage with some contribution from $s^2s^1p\sigma^1p\pi^2$, the dominant occupation of the $(2)^3\Sigma^-$ state. However, the $(2)^3\Sigma^-$ and $(1)^1\Sigma^-$ states are not coupled directly by the spin–orbit operator, so that at most only weak perturbations are expected by this crossing.

The lifetimes of the $v'=0$ and 1 levels of the $(2)^3\Sigma^+$ state are given in Table III. The bound-free transitions to the repulsive $(1)^3\Sigma^+$ and $(2)^3\Pi$ states shorten the lifetime by 6% and 13% for $v'=0$ and 1, respectively. The Franck–Condon factors for $v'=0$ are given in Table IV.

The calculated lifetimes for the $v'=0$ and 1 levels of the $(3)^3\Pi$ state are 0.595 and 0.382 μs including bound-free transitions, which do not significantly contribute to the lifetimes. The Franck–Condon factors for $v'=0$ given in Table IV indicate that the $(3)^3\Pi\rightarrow A\ ^3\Pi$ intensity will be spread over a rather broad wavelength region. While the $(3)^3\Pi\rightarrow A\ ^3\Pi$ transition makes the largest contribution to the lifetime, the similar bond lengths for the $(3)^3\Pi$ and $X\ ^3\Sigma^-$ states results in the $(3)^3\Pi\rightarrow X\ ^3\Sigma^-$ 0–0 transition having the largest A value of any of the $v'=0$ transitions. Even though the $(3)^3\Pi$–$(2)^3\Sigma^-$ separation is rather small, this transition is reasonably strong and occurs in a narrow wavelength region due to the small difference in r_e values for the two states.

TABLE V. The SA-CASSCF/ICMRCI transition moments[a] (in a.u.) at $r=3.8$, 4.0, and 4.2 a_0, computed using the ANO basis set.

Transition	3.8	4.0	4.2
$(2)^3\Sigma^- - X\ ^3\Sigma^-$	−0.044 070	0.043 548	0.177 783
$(2)^3\Sigma^- - A\ ^3\Pi$	0.063 818	0.026 336	−0.010 173
$(2)^3\Sigma^+ - A\ ^3\Pi$	0.270 446	0.238 572	0.192 728
$(2)^3\Sigma^+ - (2)^3\Pi$	0.235 809	0.286 712	0.229 411
$(2)^3\Sigma^+ - (1)^3\Sigma^+$	0.397 004	0.403 490	0.359 557
$(3)^3\Pi - X\ ^3\Sigma^-$	0.112 049	0.138 339	0.115 948
$(3)^3\Pi - A\ ^3\Pi$	0.440 040	0.029 266	−0.213 026
$(3)^3\Pi - (2)^3\Sigma^-$	0.510 111	0.396 396	0.267 845
$(3)^3\Pi - (2)^3\Pi$	0.115 814	0.243 276	0.277 800
$(3)^3\Pi - (1)^3\Sigma^+$	0.097 846	0.202 773	0.181 511
$(3)^3\Pi - (1)^3\Delta$	0.202 984	0.133 671	0.054 086
$(2)^3\Delta - A\ ^3\Pi$	0.286 905	0.272 354	0.246 304
$(2)^3\Delta - (2)^3\Pi$	0.054 655	0.185 561	0.208 404
$(2)^3\Delta - (1)^3\Delta$	0.387 142	0.430 478	0.416 761
$(3)^3\Sigma^- - X\ ^3\Sigma^-$	−0.270 494	−0.058 528	0.129 783
$(3)^3\Sigma^- - A\ ^3\Pi$	0.232 453	0.244 365	0.239 925
$(3)^3\Sigma^- - (2)^3\Sigma^-$	0.434 791	0.367 653	0.249 398
$(3)^3\Sigma^- - (2)^3\Pi$	0.007 171	−0.034 299	−0.068 875

[a]The transition moments are given in their Cartesian form; the $^3\Delta$–$^3\Pi$ moments are $\sqrt{2}$ times smaller than for complex orbitals.

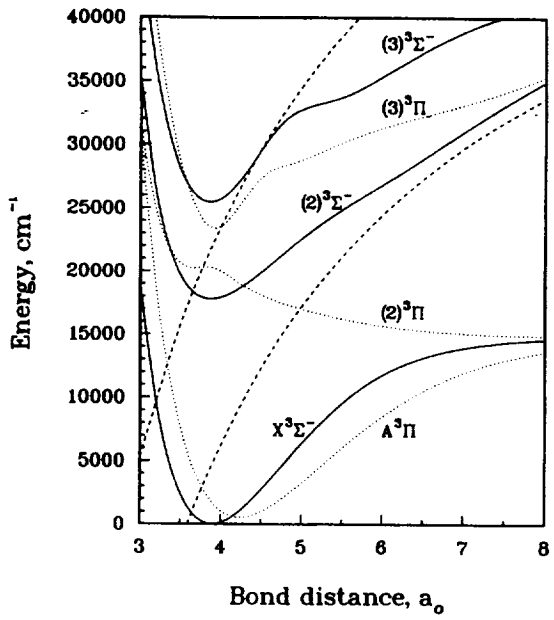

FIG. 4. The $1/r$ potential curves derived from the Al^-+B^+ and Al^++B^- asymptotes (the dashed lines) along with the $^3\Sigma^-$ states (the solid lines) and the $^3\Pi$ states (the dotted lines).

There are several decay channels for the $(2)^3\Delta$ state. The $(2)^3\Delta\rightarrow(1)^3\Delta$ bound-free transition is estimated to reduce the lifetime of the $(2)^3\Delta$ state by about 3%, whereas the bound-free $(2)^3\Delta\rightarrow(2)^3\Pi$ transition contributes little to the lifetime. The $(2)^3\Delta\rightarrow A\ ^3\Pi$ bound–bound transition is the dominant decay channel.

The radiative lifetimes of the $v'=0$ and 1 levels of the $(3)^3\Sigma^-$ state are computed to be 0.208 and 0.182 μs, respectively. While most of the decay occurs to the $A\ ^3\Pi$ state, the strongest transition from $v'=0$ is to the $v''=0$ level of the $X\ ^3\Sigma^-$ state, because of the similar bond lengths. In contrast, the significant Franck–Condon factors for transitions from the $v'=0$ level to the $A\ ^3\Pi$ state are spread over seven transitions—see Table IV. The $\Delta v=0$ transitions to the $(2)^3\Sigma^-$ state are also reasonably strong, while the repulsive $(2)^3\Pi$ state contributes very little to the lifetime.

The lowest Al^++B^- asymptote lies 5.709 eV above the ground state asymptote and gives rise to a $^3\Pi$ and a $^3\Sigma^-$ state. The second charge transfer asymptote Al^-+B^+ lies at 7.857 eV. While these ionic asymptotes are significantly higher in energy than the $^2P^\circ + {}^4P$ and $^4P + {}^2P^\circ$ asymptotes, the $1/r$ electrostatic stabilization energy places these charge transfer states at reasonably low energies; see Fig. 4 where the $1/r$ potentials derived from the Al^++B^- and Al^-+B^+ asymptotes are plotted along with the $^3\Pi$ and $^3\Sigma^-$ states. There is evidence for charge transfer states at longer r values, where the dipole moments of the $(2)^3\Sigma^-$ and $(3)^3\Pi$ states are very steep and correspond to an Al^++B^- charge distribution; this is consistent with the $1/r$ potential for this asymptote being very close to these states at large r—see Fig. 4. While these dipole moments have a large slope at longer r values, these dipole moments go to zero asymptotically, because the $^4P + {}^2P^\circ$ and $^2P^\circ + {}^4P$ asymptotes lie below the ionic limits. We also note that the $(3)^3\Sigma^-$ state has a very steep dipole moment at longer r, which corresponds to Al^-+B^+ as expected based on the $1/r$ potential derived from this asymptote. Since the computed lifetimes for the $^3\Sigma^-$ and $^3\Pi$ states of AlB are very similar to those of Al_2, the radiative lifetimes of the low-lying states do not reflect any significant charge transfer contribution. Therefore, either the charge-transfer states lie higher than those considered in this work, which is unlikely based on the plots in Fig. 4, or their contribution is spread over several states and not easily identified.

V. CONCLUSIONS

While the dissociation energy of AlB is approximately midway between B_2 and Al_2, the electronic states of AlB are observed to more closely resemble those of Al_2 than B_2. Radiative lifetimes and Franck–Condon factors are presented for several band systems to aid experimental spectroscopic studies of this molecule. The ionization potential is also computed to facilitate resonant two-photon ionization experiments. We predict that it should be possible to determine the $A\ ^3\Pi-X\ ^3\Sigma^-$ separation by observing decay from a common upper state.

[1] Z. Fu, G. W. Lemire, G. A. Bishea, and M. D. Morse, J. Chem. Phys. **93**, 8420 (1990).
[2] M. F. Cai, T. P. Dzugan, and V. E. Bondybey, Chem. Phys. Lett. **155**, 430 (1989).
[3] C. R. Brazier and P. G. Carrick, J. Chem. Phys. **96**, 8684 (1992).
[4] S. R. Langhoff and C. W. Bauschlicher, J. Chem. Phys. **92**, 1879 (1990); C. W. Bauschlicher and S. R. Langhoff, *ibid.* **90**, 4627 (1989).
[5] S. R. Langhoff and C. W. Bauschlicher, J. Chem. Phys. **95**, 5889 (1991).
[6] C. A. Arrington, T. Blume, M. D. Morse, M. Doverstål, and U. Sassenberg, J. Phys. Chem. **98**, 1398 (1994).
[7] G. Verhaegen, S. Smoes, and J. Drowart, J. Chem. Phys. **40**, 239 (1964).
[8] M. D. Morse, G. P. Hansen, P. R. R. Langridge-Smith, L.-S. Zheng, M. E. Geusic, D. L. Michalopoulos, and R. E. Smalley, J. Chem. Phys. **80**, 5400 (1984).
[9] L. Brewer, Science **161**, 115 (1968); K. Faegri and C. W. Bauschlicher, Chem. Phys. **153**, 399 (1991).
[10] G. A. Bishea, N. Marak, and M. D. Morse, J. Chem. Phys. **95**, 5618 (1991).
[11] C. W. Bauschlicher, H. Partridge, S. R. Langhoff, P. R. Taylor, and S. P. Walch, J. Chem. Phys. **86**, 7007 (1987).
[12] C. Kittel, *Introduction to Solid State Physics*, 3rd ed. (Wiley, New York, 1968), p. 78.
[13] P.-O. Widmark, J. B. Persson, and B. O. Roos, Theor. Chim. Acta **79**, 419 (1991); P.-O. Widmark, P. A. Malmqvist, and B. O. Roos, Theor. Chim. Acta **77**, 291 (1990).
[14] T. H. Dunning, J. Chem. Phys. **90**, 1007 (1989); D. E. Woon and T. H. Dunning, J. Chem. Phys. **98**, 1358 (1993).
[15] D. E. Woon, K. A. Peterson, and T. H. Dunning (personal communication); D. E. Woon and T. H. Dunning (personal communication).
[16] R. J. Gdanitz and R. Ahlrichs, Chem. Phys. Lett. **143**, 413 (1988).
[17] H.-J. Werner and P. J. Knowles, J. Chem. Phys. **89**, 5803 (1988); P. J. Knowles and H.-J. Werner, Chem. Phys. Lett. **145**, 514 (1988).
[18] H.-J. Werner and P. J. Knowles, J. Chem. Phys. **82**, 5053 (1985); P. J. Knowles and H.-J. Werner, Chem. Phys. Lett. **115**, 259 (1985).
[19] C. E. Moore, Atomic Energy Levels, Natl. Bur. Stand. (US) Circ. 467 (1949).
[20] C. W. Bauschlicher, L. A. Barnes, and P. R. Taylor, J. Phys. Chem. **93**, 2932 (1989).
[21] P. W. Deutsch, L. A. Curtiss, and J. A. Pople, Chem. Phys. Lett. **174**, 33 (1990).